Probing inter-areal computations with a cellular resolution two-photon holographic mesoscope

Lamiae Abdeladim[1*], Hyeyoung Shin[1*], Uday Jagadisan[1*], Mora B. Ogando, Hillel Adesnik[1,2,**]
[1]Department of Molecular and Cell Biology, University of California, Berkeley
[2]The Helen Wills Neuroscience Institute
* Equal contributions
** Corresponding author

Summary

Brain computation depends on intricately connected yet highly distributed neural networks. Due to the absence of the requisite technologies, causally testing fundamental hypotheses on the nature of inter-areal processing have remained largely out-of-each. Here we developed the first two photon holographic mesoscope, a system capable of simultaneously reading and writing neural activity patterns with single cell resolution across large regions of the brain. We demonstrate the precise photo-activation of spatial and temporal sequences of neurons in one brain area while reading out the downstream effect in several other regions. Investigators can use this new platform to understand feed-forward and feed-back processing in distributed neural circuits with single cell precision for the first time.

Introduction

The neural computations that support sensation, cognition and behavior depend on the precise coordination of neural activity patterns within and across widely separated brain areas. Recent advances in optogenetics and three-dimensional (3D) light patterning (Adesnik and Abdeladim 2021, Ronzitti 2017) have enabled investigators to causally probe how the activity of specific neural ensembles impact computation and drive behavior (Chettih 2019, Carillo-Reid2016, Oldenburg 2022, Marshel 2019, Dalgleish 2020, Russel 2019, Daie 2021), but only in very small, circumscribed regions of the brain on the order of <1-2mm^2. These techniques rely on phase modulation of the optical wavefront with a spatial light modulator (SLM) allowing the user to selectively target and photo-stimulate neural ensembles of interest. Despite the power of these new read/write optogenetic approaches, the inability to apply them to distributed brain networks has prevented investigators from causally probing the logic and principles of inter-areal communication that are central to brain function. A new technology that could overcome this technical barrier would allow neuroscientists to address key outstanding questions for the first time, which could have profound importance for understanding brain function in health, disease and neural development.

The recent introduction of mesoscale two photon (2p) microscopes, which can sample neural activity with near micron precision across up to 25mm^2 of brain tissue, have vastly increased the ability of investigators to acquire physiological data on distributed neural populations in behaving animals (Sofroniew 2016, Stirman 2016, Yu 2021, Rumyantsev 2020, Kim and Shnitzer 2022, Ota 2022, Machado 2022). While these 2p mesoscopes can monitor cellular activity, they have no ability to perturb it, preventing the user from probing causal relationships between the activity in connected brain areas and behavior. Thus, if it were it possible to develop a 2p mesoscope that can not only measure but also manipulate neural activity with cellular resolution, neuroscientists could use such a system to address longstanding mysteries of long-range neural communication in the brain.

However, there are multiple significant technical challenges to achieving high holographic resolution optogenetics in a 2p mesoscope. These include addressing the lower numerical aperture (NA) of the optical system and the need for mechanical rotation of the entire imaging system for accessing lateral brain areas. Furthermore, existing commercial 2p mesoscopes were not designed for the integration of holographic systems, requiring a significant redesign of the mesoscope build. To overcome these challenges, we designed and optimized a flexible 3D holographic system fully integrated onto a 2p random-access (2p-RAM) mesoscope that enables single-cell resolution holographic photo-stimulation of neural ensembles in the brain. We tested and validated the optical capabilities of this new read/write platform to measure and recreate highly specific patterns of activity in the brain within a very large FOV. In particular, we demonstrated holographic emulation of visually evoked neural activity at the mesoscale by specific co-activation of functionally defined ensembles. We further showed how one can use this system to probe functional interactions between distant brain regions. Finally, we showed that we can decode the identity of the specific photo-stimulus purely from the modulation of activity of postsynaptic neurons in downstream areas.

Together, these data illustrate how our 2P holographic mesoscope enables the user to probe causality both at the local and the interareal level with single-cell resolution. By providing the means for whole new classes of experiments, this novel technology could have a substantial impact on neuroscience research and on potential therapeutic applications.

Results

A 2P-RAM mesoscope with temporally focused 2P holographic illumination

We designed a mesoscale all-optical read/write platform around a two-photon random access (2P-RAM, Sofroniew 2016) system (**Fig 1a-c**) that is commercially available (Thorlabs, Inc.). The key features of this imaging system that make it a powerful tool for studying inter-areal communication are its nominal 5x5mm FOV, a fast remote focusing system for FOV curvature correction and multiplane imaging, and four automated axes of motion for positional flexibility (**Fig1c**). We sought to develop a mesoscale holographic optogenetics system that achieves single cell resolution photo-stimulation despite the lower numerical aperture of the optical path and that could likewise address the imaging plane curvature. Furthermore, we aimed for an optical design that does not compromise the 4-axis movement capabilities of the 2P-RAM system, since they are essential for executing a diverse array of neurobiological experiments. We therefore designed a compact and re-dimensioned 3D holographic module that employs temporal focusing to confine excitation axially ('3D-SHOT', three-dimensional sparse holographic optogenetics with temporal focusing Mardinly 2018, Pégard 2017). To preserve all translational axes of the entire system, we built the holographic module on an extension breadboard attached to the movable main frame of the microscope (**Fig1b**). In 3D-SHOT, an initial blazed grating generates a temporally focused disc of light that is magnified and replicated in multiple locations within a 3D volume by a spatial light modulator (SLM). The 3D light pattern is then relayed onto the objective image space through a set of 4f-systems (**Fig 1c,**). Given the large distance on the mesoscope between the photostimulation laser output and the 3D-SHOT module, we added a non-magnifying telescope after the laser to control the divergence of the beam impinging on the diffraction grating. Preserving the alignment invariance of the holographic path with the motorized movements of the mesoscope is a key challenge. To address this (**Fig1c**), we first combined the imaging and photostimulation beam before entering the multi-stage periscope so that the photostimulation beam maintains invariance with X and Y frame translations. Second, we replaced the last periscope mirror with a long-pass dichroic that directs the imaging beam (920nm) onto the vertical breadboard and the photostimulation beam (1030nm) onto the extension breadboard so that the latter

maintains invariance with rotation. Third, we recombined both beams with a short-pass dichroic placed right before the mesoscope tube lens on the vertical breadboard. Consequently, the holographic module is invariant within all dimensions controlled by the motorized microscope frame, X, Y translations and rotation. We recovered axial translation by adding a motorized stage for animal positioning along the vertical axis, additionally mounted on a goniometer to ensure that imaging and photo-stimulation are fully orthogonal to the cranial window surface.

To quantify the optical resolution of the mesoscale holographic system, we first measured the spatial profile or 'point spread function' (PSF) of single two photon excitation spots (**Fig 1d-e**) which measured 9µm in the lateral dimension and 32µm in the axial dimension (**Fig 1g**). Although these values are slightly larger than those previously reported for 3D-SHOT in a conventional 2p microscope, they are consistent with the modestly lower NA of the mesoscope objective. Nevertheless, the range of optical PSFs across the entire photostimulation field is within the range of optical PSFs reported in previous single-cell 2P holographic optogenetics studies (Pegard 2017, Mardinly 2018, Packer 2012) and allows for quasi single-cell resolution targeted photostimulation. We then determined the extent of our holographic field-of-view (FOV) which is equivalent to the total accessible FOV range of the SLM at the system's magnification. We set the FOV limits to the farthest accessible holograms without aliasing which corresponded to a total lateral FOV of ~1mm × 1mm (**Fig. 1g**), on par with the expected theoretical FOV limit xx. Next, we generated multiple holograms spatially arranged in a 3D point-cloud (**Fig 1f**). For these holograms, the measured axial optical PSFs were mostly invariant within a digital defocusing range of 220 µm (**Fig 1h**).

Finally, we assessed holographic targeting stationarity with X, Y translations and rotation, which is essential for accurate optical generation of neural activity patterns despite movement of the mesoscope relative to the brain. We found that the error between original hologram location and at displaced stage positions remained less than 2 µm over a ± 3mm translation range and a ± 2.5° rotation angle range demonstrating alignment invariance with mesoscope frame movements.

In vivo 2P photostimulation on the 2P-RAM mesoscope

Next, we tested our system for *in vivo* all-optical control of neural ensembles in awake mice. We took advantage of a transgenic line that we recently developed (Vglut1-Cre;Ai203) (Bounds, 2021) which provides widespread and stable co-expression of the potent opsin ChroME and the sensitive calcium indicator (GCaMP7s) (**Fig. 2a**). We were able to photoactivate selected individual cells within the holographic FOV while recording from thousands of neurons within the mesoscale imaging FOV (**Fig. 2b-e**). Sequential photostimulation at 75mW/spot (10 × 10 ms pulses **at 50Hz**) elicited significant time-locked responses in 70% of targeted cells (**Fig. 2c**,**d**). This demonstrates effective holographic photostimulation despite the increased group-delay dispersion from the mesoscope refractive optics (mostly the large mesoscope objective) and the slightly larger optical axial resolution. To carefully quantify the effective spatial resolution of holographic photo-stimulation, we recorded physiological point-spread-functions (PPSFs) all optically in awake animals. We estimated the lateral PPSF to be 23 µm and the axial PSF to be 49 µm (gaussian fit full-width-half-maximum, n=3 cells). Despite the lower NA inherent to the mesoscope objective, the achieved effective axial resolution *in vivo* is even lower than some reported PPSFs in 2p optogenetics studies (Daie 2021). This was achieved mainly by reducing the effective lateral size of our temporally-focused disk while still maintaining enough cell coverage for efficient photoactivation. Together, these results demonstrate that the 2p holographic mesoscope achieves single-cell resolution holographic optogenetics on par with previous implementations on conventional 2P microscopes.

To illustrate how one can use the 2P holographic mesoscope to address key questions related to inter-areal processing, we sequentially targeted ensembles of neurons in different visual areas while recording the same set of visual cortical areas via translation of the mesoscope, taking advantage of the system's targeting invariance to spatial translation. We could thus sequentially activate neural ensembles from four different cortical areas (V1, PM, RL, and LM) while simultaneously recording activity from six surrounding visual areas (**Fig. 2f**). Indeed, photo-stimulation in each cortical area elicited robust response in the holographically targeted cells even while we maintained acquisition of physiological data from the entire FOV. This demonstrates that the new system achieves ensemble stimulation in any chosen visual area while concurrently recording neural activity from thousands of neurons in surrounding visual areas.

Holographic stimulation of functionally defined ensembles at the mesoscale

A major advantage of two-photon holographic optogenetics is the ability to co-activate ensembles of neurons based on their functional properties. We thus asked if we could co-activate groups of visual cortical neurons that share orientation preference (**Fig. 3**). In the mouse visual cortex, orientation preference shows minimal spatial clustering and thus co-activating an ensemble of co-tuned neurons required highly precise optical targeting. To test this capability, we measured orientation tuning curves of V1 neurons and then constructed various ensembles of neurons with shared orientation preference for 2p holographic stimulation (**Fig. 2b,c**). Indeed, we could successfully photo-activate groups of co-tuned neurons in V1 (**Fig 2d**.) while recording activity from surrounding areas. To test whether our holographic stimulation generated functionally specific patterns of neural activity, we trained a decoder to discriminate between responses evoked by static gratings in 4 orientations. In the test phase, we then asked the decoder to assign responses evoked by photostimulation of co-tuned ensembles to the 4 orientations to the appropriate visual stimulus. The decoder was able to classify holographic photo-stimuli above chance across both targets and all recorded neurons (**Fig. 3 f,g**), demonstrating emulation of visually evoked activity.

Mesoscale recording of long-range responses to holographic neural activation

One of the major advantages of mesoscale two-photon holographic optogenetics should be the ability to detect and quantify long-range functional interactions between one area and several other brain areas simultaneously, something not possible with conventional 2p microscopes. To test this, we stimulated ensembles of neurons in visual area LM while recording from neurons across 4-6 other visual cortical areas in a total 3 mm × 1.8 mm FOV or 2.4 mm × 2.4 mm FOV at 5Hz and 4.5Hz respectively. We detected both reliably activated and reliably suppressed neurons downstream (**Fig. 4a-c**). As a control, we compared the distribution of significant responses in stimulation trials with the significant responses on 'catch trials' where photo-stimulation power was set to 0mW (**Fig. 4b**) and showed that holographic stimulation induces postsynaptic modulation above the statistical false positive rate(**Fig. 4b**). We next quantified the net modulatory effect of LM photo-activation on the other imaged visual areas as well as well area LM itself, excluding cells less than 50 µm from the holographic targets. We observed a significant albeit modest suppression of mean activity across all downstream areas, with LM neurons showing the strongest suppression and PM neurons showing the least.

Finally, we asked if activating different neural activity patterns in one cortical area (LM) induces differentiable patterns of modulation in downstream areas. To test this idea, we used machine learning

algorithms to decode, trial by trial, the identity of the holographically induced pattern in LM from the neural responses in the other visual areas (**Fig. 4f,g**). Indeed, we could properly predict the holographic pattern on each trial significantly above chance levels, despite excluding all measurements taken from LM itself. This indicates that photostimulation of even relatively modestly size neural ensembles is sufficient to drive distinct, distributed and informative patterns of neuromodulation downstream at the cellular scale.

Discussion

We designed, built and validated a the first multiphoton holographic mesoscope. This technology is the first to offer targeted photostimulation with single-cell resolution with simultaneous large-scale recording of neural activity across several cortical areas in a nominal 25mm^2 FOV. We demonstrated the new system's ability to co-activate user-defined groups of neurons, selected based on their spatial or functional properties, while simultaneously recording neural activity from several downstream areas. We could identify individual downstream neurons that displayed time-locked excitatory or inhibitory responses hundreds or even thousands of microns away. This demonstrates that one can use this new technology to probe how both local and long-range functional interactions relate to specific neuronal computations all within the same experiment.

We developed the mesoscale read/write platform based on a commercially available 2p mesoscope (Thorlabs) that is a widely used mesoscope platform (cite some studies) and that has enabled a number of other recent technological advances (Lu 2020, Demas 2021, Tsyboulski 2018). We expect that adapting a commercially available system will facilitate the adoption of the technology across both individual labs and new neurotechnology platforms. In the current design, the holographic FOV is limited by the SLM accessible FOV which, given the system's current magnification is in the millimetric range. Extending the holographic FOV to the entire mesoscale nominal FOV of the objective can be achieved by serially combining two conjugated SLMs, combining one SLM and one galvanometer mirror (Sun 2019), or spatially tiling multiple SLMs (Marshel 2019, Yang 2015), albeit at the cost of increased setup complexity. Nevertheless, the current configuration is sufficient to answer many fundamental outstanding questions in cortical function.

One recent study investigated inter-areal communication using a conventional two-photon microscope by imaging across the boundary of two contiguous cortical regions (Rowland 2021). The mesoscale platform presented here allows access to up to up to 25-fold more cortical surface (albeit at lower frame rates or lower spatial sampling). This much larger FOV encompasses many more cortical areas, more coverage of feature-space within selected areas and the ability to study non-contiguous areas that are more than 1mm apart.

While there is substantial work detailing how individual cortical areas represent and encode information, how neural representations are transformed across cortical areas remains elusive. Most studies addressing cortico-cortical communication combined multi-site electrode recordings with correlative analyses (Bressler 2011, Semedo 2019), or electrical or one-photon optogenetic stimulation. However, electrical microstimulation provides limited spatial control and often (and perhaps preferentially) activates axons of passage (Histed 2009). One-photon optogenetic stimulation has cell-type specific control but cannot readily activate functional defined subsets of neurons (such as neurons with the same feature preference). Neither stimulation approach can recreate precise spatiotemporal sequences of activity, nor can they drive different user-defined firing rates into different neurons to recreate specific population activity vectors that might preferentially drive cortico-cortical communication (Semedo 2019).

2p holographic optogenetics can achieve these goals (Bounds 2017, Mardinly 2018), and this new 2p holographic mesoscope can implement these perturbations while simultaneously measuring both local and downstream neural activity. Thus, 2p mesoscale holography is set up to experimentally test major hypotheses and theories of interareal communication, such as how cortico-cortical feedback implements generative models of the external world such as in the framework as predictive coding (Rao and Ballard 1999, Markov and Kennedy 2013, Hertag and Clopath 2022). The 3D capability of the mesoscale read/write platform both in photostimulation (3D-SHOT) and recording (3D remote focusing) can further allow the user to test the role of different cortical layers in these models (Bastos 2012).

Previously, we showed that photostimulation with 3D-SHOT and potent and fast optogenetic proteins enables millisecond-precise recreation of neural activity sequences across large ensembles of neurons (Sridharan, 2022). The 2p mesoscope we developed should have similar capabilities since it also employs 3D-SHOT, although this is difficult to validate directly with in-vivo electrophysiology due to the bulky size of the objective. Several prominent theories of cortico-cortical communication, and inter-areal communication more generally, depend on the synchrony and/or oscillatory timing of activity in the sender and receiver area (Bastos 2015). We expect that this 2p holographic mesoscope should be capable of generating precise temporal sequences of neural activity in one area while monitoring the net impacts downstream. If so, it should be possible to ask directly how synchrony or oscillatory coherence facilitate communication, potentially in different frequency bands, between hierarchically organized brain areas.

The 2P holographic mesoscope could also guide the design of more effective brain-machine interfaces (BMIs, Ersaro 2023). Signal transmission across areas can be iteratively optimized with single-cell resolution and millisecond precision by identifying and testing optimal communication subspaces for signal flow (Semedo, 2019) and/or dynamically adjusting spiking coordination. Obtaining access to intermediate stages of processing between the perturbed population activity and behavioral output should help optimize the photostimulation patterns that can maximize the fidelity of robotic limb control. In the context of limb neuroprosthetics (Lebedev and Nicolelis, 2006), mesoscale 2P holography could further incorporate fine tactile and proprioceptive-like feedback signals into the BMI that could make prostheses seamlessly fit as a natural limb extension.

Finally, the large accessible FOV of the mesoscope will help scale two-photon optogenetics to species with larger brains such as primates. It can also enable new experimental paradigms in species smaller than the mouse, such as larval zebrafish, where one could perform targeted photostimulation in the central nervous system (CNS) while recording from both the CNS and peripheral organs. It could even allow photo-stimulation and recording from multiple small animals simultaneously, such as flies or worms, engaged in social behaviors. Overall, we expect mesoscale two-photon holographic optogenetics to become a key technology in systems neuroscience because it can establish whole new classes of perturbative experiments to motivate and test previously untestable theories of brain function.

Acknowledgements

This work was funded by NIH grants R01NS128772, UF1NS107574, and R01MH117824. H.A. is a Chan Zuckerberg Biohub Investigator.

Author contributions

L.A. and H.A. conceived of the project. L.A. designed and built the 2p holographic system with assistance from Thorlabs. L.A and U.K.J characterized the system. L.A., H.S. and U.K.J. performed

experiments. M.O contributed software. L.A. and H.A. wrote the paper with assistance from H.S. and U.K.J.

References

Adesnik, H., & Abdeladim, L. (2021). Probing neural codes with two-photon holographic optogenetics. *Nature neuroscience*, *24*(10), 1356-1366.

Akturk, S., Gu, X., Kimmel, M., & Trebino, R. (2006). Extremely simple single-prism ultrashort-pulse compressor. *Optics express*, *14*(21), 10101-10108.

Bastos, A. M., Usrey, W. M., Adams, R. A., Mangun, G. R., Fries, P., & Friston, K. J. (2012). Canonical microcircuits for predictive coding. *Neuron*, *76*(4), 695-711.

Bastos, A. M., Vezoli, J., & Fries, P. (2015). Communication through coherence with inter-areal delays. *Current opinion in neurobiology*, *31*, 173-180.

Botcherby, E. J., Juškaitis, R., Booth, M. J., & Wilson, T. (2008). An optical technique for remote focusing in microscopy. *Optics Communications*, *281*(4), 880-887.

Bounds, H. A., Sadahiro, M., Hendricks, W. D., Gajowa, M., Oldenburg, I. A., Gopakumar, K., ... & Adesnik, H. (2021). Multifunctional Cre-dependent transgenic mice for high-precision all-optical interrogation of neural circuits. *bioRxiv*.

Bressler, S. L., & Seth, A. K. (2011). Wiener–Granger causality: a well established methodology. *Neuroimage*, *58*(2), 323-329.

Carrillo-Reid, L., Yang, W., Bando, Y., Peterka, D. S., & Yuste, R. (2016). Imprinting and recalling cortical ensembles. *Science*, *353*(6300), 691-694.

Chettih, S. N., & Harvey, C. D. (2019). Single-neuron perturbations reveal feature-specific competition in V1. *Nature*, *567*(7748), 334-340.

Daie, K., Svoboda, K., & Druckmann, S. (2021). Targeted photostimulation uncovers circuit motifs supporting short-term memory. *Nature neuroscience*, *24*(2), 259-265.

Dalgleish, H. W., Russell, L. E., Packer, A. M., Roth, A., Gauld, O. M., Greenstreet, F., ... & Häusser, M. (2020). How many neurons are sufficient for perception of cortical activity?. *Elife*, *9*, e58889.

Demas, J., Manley, J., Tejera, F., Barber, K., Kim, H., Traub, F. M., ... & Vaziri, A. (2021). High-speed, cortex-wide volumetric recording of neuroactivity at cellular resolution using light beads microscopy. *Nature Methods*, *18*(9), 1103-1111.

Ersaro, N. T., Yalcin, C., & Muller, R. (2023). The future of brain–machine interfaces is optical. *Nature Electronics*, 1-3.

Garrett, M. E., Nauhaus, I., Marshel, J. H., & Callaway, E. M. (2014). Topography and areal organization of mouse visual cortex. *Journal of Neuroscience*, *34*(37), 12587-12600.

Hertäg, L., & Clopath, C. (2022). Prediction-error neurons in circuits with multiple neuron types: Formation, refinement, and functional implications. *Proceedings of the National Academy of Sciences*, *119*(13), e2115699119.

Histed, M. H., Bonin, V., & Reid, R. C. (2009). Direct activation of sparse, distributed populations of cortical neurons by electrical microstimulation. *Neuron*, *63*(4), 508-522.

Juavinett, A. L., Nauhaus, I., Garrett, M. E., Zhuang, J., & Callaway, E. M. (2017). Automated identification of mouse visual areas with intrinsic signal imaging. *Nature protocols*, *12*(1), 32-43.

Kim, T. H., & Schnitzer, M. J. (2022). Fluorescence imaging of large-scale neural ensemble dynamics. *Cell*, *185*(1), 9-41.

Lebedev, M. A., & Nicolelis, M. A. (2006). Brain–machine interfaces: past, present and future. *TRENDS in Neurosciences*, *29*(9), 536-546.

Lu, R., Liang, Y., Meng, G., Zhou, P., Svoboda, K., Paninski, L., & Ji, N. (2020). Rapid mesoscale volumetric imaging of neural activity with synaptic resolution. *Nature methods*, *17*(3), 291-294.

Machado, T. A., Kauvar, I. V., & Deisseroth, K. (2022). Multiregion neuronal activity: the forest and the trees. *Nature Reviews Neuroscience*, *23*(11), 683-704.

Mardinly, A. R., Oldenburg, I. A., Pégard, N. C., Sridharan, S., Lyall, E. H., Chesnov, K., ... & Adesnik, H. (2018). Precise multimodal optical control of neural ensemble activity. *Nature neuroscience*, *21*(6), 881-893.

Markov, N. T., & Kennedy, H. (2013). The importance of being hierarchical. *Current opinion in neurobiology*, *23*(2), 187-194.

Marshel, J. H., Garrett, M. E., Nauhaus, I., & Callaway, E. M. (2011). Functional specialization of seven mouse visual cortical areas. *Neuron*, *72*(6), 1040-1054.

Marshel, J. H., Kim, Y. S., Machado, T. A., Quirin, S., Benson, B., Kadmon, J., ... & Deisseroth, K. (2019). Cortical layer–specific critical dynamics triggering perception. *Science*, *365*(6453), eaaw5202.

Oldenburg, I. A., Hendricks, W. D., Handy, G., Shamardani, K., Bounds, H. A., Doiron, B., & Adesnik, H. (2022). The logic of recurrent circuits in the primary visual cortex. *bioRxiv*, 2022-09.

Ota, K., Uwamori, H., Ode, T., & Murayama, M. (2022). Breaking trade-offs: Development of fast, high-resolution, wide-field two-photon microscopes to reveal the computational principles of the brain. *Neuroscience Research*, *179*, 3-14.

Pachitariu, M., Stringer, C., Schröder, S., Dipoppa, M., Rossi, L. F., Carandini, M., & Harris, K. D. (2016). Suite2p: beyond 10,000 neurons with standard two-photon microscopy. *BioRxiv*, 061507.

Packer, A. M., Peterka, D. S., Hirtz, J. J., Prakash, R., Deisseroth, K., & Yuste, R. (2012). Two-photon optogenetics of dendritic spines and neural circuits. *Nature methods*, *9*(12), 1202-1205.

Pégard, N. C., Mardinly, A. R., Oldenburg, I. A., Sridharan, S., Waller, L., & Adesnik, H. (2017). Three-dimensional scanless holographic optogenetics with temporal focusing (3D-SHOT). *Nature communications*, *8*(1), 1228.

Rao, R. P., & Ballard, D. H. (1999). Predictive coding in the visual cortex: a functional interpretation of some extra-classical receptive-field effects. *Nature neuroscience*, *2*(1), 79-87.

Ronzitti, E., Ventalon, C., Canepari, M., Forget, B. C., Papagiakoumou, E., & Emiliani, V. (2017). Recent advances in patterned photostimulation for optogenetics. *Journal of Optics*, *19*(11), 113001.

Rowland, J. M., van der Plas, T. L., Loidolt, M., Lees, R. M., Keeling, J., Dehning, J., ... & Packer, A. M. (2021). Perception and propagation of activity through the cortical hierarchy is determined by neural variability. *bioRxiv*, 2021-12.

Rumyantsev, O. I., Lecoq, J. A., Hernandez, O., Zhang, Y., Savall, J., Chrapkiewicz, R., ... & Schnitzer, M. J. (2020). Fundamental bounds on the fidelity of sensory cortical coding. *Nature*, *580*(7801), 100-105.

Russell, L. E., Yang, Z., Tan, P. L., Fişek, M., Packer, A. M., Dalgleish, H. W., ... & Häusser, M. (2019). The influence of visual cortex on perception is modulated by behavioural state. *biorxiv*, 706010.

Semedo, J. D., Zandvakili, A., Machens, C. K., Byron, M. Y., & Kohn, A. (2019). Cortical areas interact through a communication subspace. *Neuron*, *102*(1), 249-259.

Sofroniew, N. J., Flickinger, D., King, J., & Svoboda, K. (2016). A large field of view two-photon mesoscope with subcellular resolution for in vivo imaging. *elife*, *5*, e14472.

Sun, S., Zhang, G., Cheng, Z., Gan, W., & Cui, M. (2019). Large-scale femtosecond holography for near simultaneous optogenetic neural modulation. *Optics express*, *27*(22), 32228-32234.

Stirman, J. N., Smith, I. T., Kudenov, M. W., & Smith, S. L. (2016). Wide field-of-view, multi-region, two-photon imaging of neuronal activity in the mammalian brain. *Nature biotechnology*, *34*(8), 857-862.

Sridharan, S., Gajowa, M. A., Ogando, M. B., Jagadisan, U. K., Abdeladim, L., Sadahiro, M., ... & Adesnik, H. (2022). High-performance microbial opsins for spatially and temporally precise perturbations of large neuronal networks. *Neuron*, *110*(7), 1139-1155.

Tsyboulski, D., Orlova, N., Griffin, F., Seid, S., Lecoq, J., & Saggau, P. (2018). Remote focusing system for simultaneous dual-plane mesoscopic multiphoton imaging. *BioRxiv*, 503052

Yang, S. J., Allen, W. E., Kauvar, I., Andalman, A. S., Young, N. P., Kim, C. K., ... & Deisseroth, K. (2015). Extended field-of-view and increased-signal 3D holographic illumination with time-division multiplexing. *Optics express*, *23*(25), 32573-32581.

Yu, C. H., Stirman, J. N., Yu, Y., Hira, R., & Smith, S. L. (2021). Diesel2p mesoscope with dual independent scan engines for flexible capture of dynamics in distributed neural circuitry. *Nature communications*, *12*(1), 6639.

Zhuang, J., Ng, L., Williams, D., Valley, M., Li, Y., Garrett, M., & Waters, J. (2017). An extended retinotopic map of mouse cortex. *elife*, *6*, e18372.

Methods

Animals

All experiments on animals were conducted with approval of the Animal Care and Use Committee of the University of California, Berkeley. All experiments were performed in mice of both sexes, aged two months and older. Two transgenic mouse lines were used: either Ai203 transgenic lines (Bounds et al) crossed in house with Vglut1-Cre mice, or triple transgenic mice emx1-Cre;CaMK2-tTA;tetO-GCaMP6s obtained by crossing the corresponding lines in-house (JAX stock# 005628, Jax stock# 003010 and Jax stock# 024742). Mice were housed in groups of five or fewer in a reverse light: dark cycle of 12:12 hours. Experiments were conducted during the dark phase.

Surgery

Mice were anesthetized with isoflurane (2%) and given buprenorphine as an analgesic (0.05mg/kg) and dexamethasone (2mg/kg) to reduce brain swelling. Mice were then placed in a stereotaxic frame (Kopf) over a heating pad. The scalp was removed, the fascia pushed to the sides, and the skull lightly scratched for better cement adhesion. A 4 or 5mm craniotomy centered around V1 was made using a biopsy punch (Robbins Instruments) and/or a dental drill (Foredom). Bleeding was controlled with cold phosphate-buffered saline and Gelfoam (Pfizer Inc.) For mice that required viral injection (triple transgenics), the virus preparation (AAV9-CAG.DIO.ChroME2s-FLAG-ST.P2A.H2B.mRuby3.WPRE.SV40) was injected using a beveled glass pipette at 4-5 locations across visual cortex. A cranial window, made of 7 mm and 5 mm diameter glass coverslips or 6 mm and 4 mm diameter glass coverslips, for 5 and 4 mm craniotomies respectively, was then placed onto the craniotomy and held in place with Metabond (C&B). Finally, a titanium headplate was fixed to the skull with Metabond (C&B0 and Ortho Jet (Lang). All craniotomies were performed on the left hemisphere of the mouse brain. Animals were allowed to recover in a heated recovery cage before being returned to their home cage.

2P-RAM mesoscope with a temporally-focused holographic path

The mesoscale read/write platform was custom-built around a 2P random-access fluorescence mesoscope previously described in detail (Sofroniew 2016l) and now commercialized by Thorlabs Inc. The system had a nominal 5mm FOV accessed through a 0.6 NA objective that can be rapidly and flexibly scanned-across with a set of four conjugated scanners, one 12kHz resonant scanner and three large-angle galvanometers. The system was also equipped with a voice-coil remote-focusing module (Botcherby 2008) for 3D multi-plane imaging. In addition, the mesoscope was built on a vertical breadboard and the whole system was motorized in 4 dimensions (X, Y, Z translation and one axis of rotation) to provide maximal flexibility for the user. Since the microscope moved with respect to the incoming laser beam, the beam was injected through a six-stage periscope for alignment invariance.

The 2P mesoscale imaging path relied on a Ti:sapphire laser (Mai Tai, Spectra Physics) used at 920 nm for calcium imaging. External power control was achieved through a Pockels cells (Conoptics, Inc). A prism-based group delay dispersion compensation module (Akturk 2006) was installed to compensate for dispersion introduced by the mesoscope imaging path optics (estimated at about 25,000 fs^2 , Sofroniew 2016). The 2P holographic path relied on a 1030 nm femtosecond fiber laser (Aeropulse 50, NKT Photonics) with internal power control.

The holographic path was built on a 33”” × 24”” breadboard attached to the main mesoscope frame with three custom mounts. The holographic beam was merged with the imaging beam with a 1000 nm cutoff dichroic (DMSP1000R, Thorlabs) and rigorously co-aligned with the imaging beam through the system’s

periscope to maintain alignment invariance with translation. The beam was then injected onto the 3D-SHOT optical path with specific care to maintaining beam horizontality to achieve alignment invariance with rotation.

The imaging path hardware was controlled with ScanImage software (Vidrio Technologies,LLC). Custom Matlab code was used for control of the photostimulation path hardware, synchronization with imaging and control of the visual stimulation.

Hologram characterization and system calibration

To characterize the generated holograms, 2P fluorescence was recorded from a thinly coated fluorescent slide with a substage objective (×4 Zeiss) coupled to a camera (Basler) with a f=125 mm achromatic doublet which provided a 1.3 × 1.3 mm characterization FOV. For successful multiphoton optogenetics experiments, precise co-alignment of the imaging and the photostimulation beams is required. To achieve this, hundreds of holograms were generated in 3D and any arbitrary curvature or inhomogeneity on the imaging remote-focusing planes or the SLM planes was taken into account in the computation of the hologram to real space transform matrix, in a fully automated procedure (Oldenburg 2022). The holographic FOV was then remapped onto the entire mesoscopic FOV so that photostimulation targets could be flexibly selected in any imaging ROI configuration. The recorded holograms were also used as a reference to correct for diffraction efficiency fall-off and deliver homogeneous powers across the field-of-view *in-vivo*. To characterize hologram position invariance with translation and rotation, 2D point-cloud holograms were generated to “burn holes” i.e photobleach a fluorescent slide. The 2P fluorescence signal on the slide was then recorded with the mesoscope photomultiplier tubes (PMTs).

Visual stimulation and retinotopy

Visual stimuli were displayed on a 2048 × 1536 Retina iPad LCD monitor (Adafruit Industries) placed 10 cm from the right eye of the mouse, and computed using Psychtoolbox-3 and custom MATLAB code. Visual stimuli were presented to map retinotopy and to identify functionally-defined ensembles. Otherwise, no visual stimulus was presented to the mouse during simultaneous imaging and photostimulation experiments.

Retinotopy mapping was used primarily to identify visual cortical area boundaries. To map retinotopy, we adapted the procedure used in Marshel, et al., 2011 and Zhuang, et al., 2017 for the 2-photon mesoscope. Briefly, we imaged a 3.1 x 3.1mm FOV 100-200um below the dura at 3Hz when mice were viewing noise bars drifting in the horizontal or vertical directions. The bars were 10’ in width and spanned the vertical or horizontal extents of the screen respectively. The noise was drawn from a gaussian distribution with spatial frequency 0.03 cycles/deg and temporal frequency 3 cycles/deg. Each type of bar swept the screen 30 times with a period of 9s, for a total stimulation duration of 10 minutes. We smoothed the recorded 2-photon calcium frames with a 4-8 pixel square filter and downsampled them by 4-8x. For each pixel in the reduced image, we computed the preferred azimuth and elevation by identifying the average horizontal and vertical positions of the bar at which the pixel’s response was maximal. This generated azimuth and elevation preference maps for the full FOV. We then computed the sign of the gradients between the two maps to generate a visual field sign map (Sereno, et al., 1994), and used sign flips in this map to identify area boundaries as outlined in (Garrett, et al., 2014, Juavinett, et al., 2017).

In vivo mesoscale two-photon imaging and photostimulation

For *in vivo* 2-photon mesoscale calcium imaging in vivo, mice were head-fixed and allowed to run on a freely moving 768 circular treadmill. Mesoscale Imaging ROIs were set to 2.4 × 2.4 mm to 3.6 mm × 3.6

mm FOVs with recording rates between 3 and 5Hz. The imaging laser was set at 920 nm. Opsin expressing cells were automatically segmented online based on either the green channel signal (Ai203 mice) or the red nuclear mRuby2 (virally injected mice).

Optical physiological point-spread function measurements

To estimate the PPSF, we first identified photoactivatable neurons near the center of the holography FOV and selected 8 targets for multi-target stimulation. We generated 50 8-target holograms around and including the central holograms, 17 for the lateral PPSF and 33 for the axial PPSF. For the lateral PPSF, each hologram was offset in the [-40,40] um range with 5um increments along the x-axis. For the axial PPSF, each hologram was offset in the [-80,80] um range with 5 um increments along the z-axis. Each hologram was illuminated with 5 x 5ms pulses @ 30Hz and 25mW/target, with 10 repeats per hologram. The responses of the targeted neurons was averaged over each condition's repeats to compute the PPSF.

Multi-area targeting

For the multi-area holography demonstration in Figure 2f, we first identified area boundaries using retinotopy, and picked 4 visual cortical areas (V1, PM, RL, and LM) for same-session sequential targeting. For each area, we moved the objective along both lateral axes until the holographic FOV (fixed with respect to the objective) was positioned over the center of the area. We then adjusted the 2P-RAM scanfields to image a contiguous 3.1 x 3.1 mm area covering a fixed portion of the window using the vasculature as fiduciary markers. As a result, at the beginning of each area's experiment, the imaging FOV was identical, but the holography FOV covered a different cortical area. In each experiment, we identified 10-15 of the most photoactivatable neurons with sequential single-neuron targeting. We then targeted these neurons (V1-13, PM-12, RL-11, LM-12 neurons) in each area using a multi-target hologram, driving them with a single 250ms pulse and 80 mW per target.

Holographic Stimulation of Functionally Defined Ensembles

For co-tuned ensemble stimulation experiments presented in Figure 3, we used Vglut1-Cre;Ai203 mice (Ai203 refers to a transgenic line expressing the transgene TITL-st-ChroME-GCaMP7s-ICL-nls-mRuby3-IRES2-tTA2; Bounds et al., 2022). We recorded 11 sessions from 2 female mice (5 and 6 sessions each mouse). The holographic FOV was placed over V1 (white rectangle in Figure 3a). The imaging FOV encompassed V1, LM, RL, AL, PM and AM (2400 X 2400 m2). The imaging and holographic FOV was fixed throughout each recording session.

To holographically stimulate neural ensembles defined by their visual response properties, each recording session consisted of 3 steps. In Step 1, we recorded visual responses of neurons in the FOV while the mouse viewed various images on the monitor. To gauge the orientation preference of each neuron, we presented static gratings in 4 different orientations (0, 45, 90, 135°), at a contrast of 0.75 and spatial frequency of 0.04 cycles per degree. Gray screen 'blank' trials, as well as static gratings in each orientation, was repeated 50 times, with randomized trial order. Each presentation, or trial, lasted for 1 s with 0 s inter-trial intervals. As such, the static grating block lasted 250 s (5 trial types X 50 repeats X 1s duration). In the Step 2, we analyzed the 2p imaging data collected in Step 1 by running Suite2p on the computer where ScanImage was running. Before running Suite2p, we converted the ScanImage tif files into an h5 file as follows: 1) loading the ScanImage tif files; 2) cropping it into region corresponding to the holographic FOV; 3) keeping only the frames corresponding to the functional channel (e.g., every other frame if both red and green PMTs were recorded); and 4) saving as an h5 file. It was important to convert at least 5000 time points, because Suite2p identifies many more spurious ROIs with shorter recordings.

Next, we ran Suite2p on the cropped h5 file. Because there is insufficient time to manually curate the ROIs during the online analysis, we analyzed tuning curves for every ROI returned by the Suite2p. In Step 3, we holographically stimulated neural ensembles defined in Step 2. Each target received 50mW, and each stimulation consisted of 10 pulses of 10 ms duration at 16 Hz. In addition to the co-tuned ensemble stimulation at 4 orientations, 0-power 'blank' trials and mixed-tuned ensemble stimulation trials were interleaved (i.e., 6 trial types). Each trial type was repeated 20 times with an inter-trial interval of 5 s.

Holographic Stimulation of random multi-target ensembles

For the targeted photostimulation experiment presented in Figure 4a-c, we used virally injected transgenic mice (EMX1-Cre;CaMK2-tTA;tetO-GCaMP6s injected with AAV9-CAG.DIO.ChroME2s-FLAG-ST.P2A.H2B.mRuby3.WPRE.SV40). The holographic FOV was placed over LM. The imaging FOV encompassed V1, LM, RL, PM and AM (2400 X 2400 µm2). Stimulation consisted of long 250ms pulses, at zero power, P=30mW and P=50mW, with 200 trials per power condition to maximize detectability of long-range responses. P=30mW and P=50mW trials were averaged as the stimulation condition.

For the targeted photostimulation experiments presented in Figure 4d-g, we used Vglut1-Cre;Ai203 mice. We recorded 4 sessions from 2 female mice (n=2 sessions each). The holographic FOV was placed over LM. The imaging FOV encompassed V1, LM, RL, AL, A and AM (3000 X 1800 µm2). Each target received 50mW, and each stimulation consisted of 10 pulses of 10 ms duration at 16 H. In each session, 4 distinct holograms were used in addition to a zero power condition, with 80 trials per condition.

Offline analysis of mesoscopic two-photon calcium data

Motion correction and source extraction were done using Suite2p (Pachitariu, 2016), run through GPU for faster processing. Calcium sources were manually curated based on morphologically identifiable neurons. For downstream analysis, frames with stimulation laser artefacts were discarded and neuropil fluorescence was subtracted from the fluorescence traces using a 0.7 neuropil coefficient. Each cell's fluorescence trace was then z-scored (Figure 2) or the dF/F was computed prior to z-scoring (z-scored dF/F). dF/F was defined as (F-Fmed)/Fmed where F is the neuropil corrected fluorescence trace and Fmed the median of the neuropil corrected fluorescence trace across all trials. A baseline of 2-5 frames before the stimulus onset was then subtracted for every trial (Figures 3,4). In long-range post-synaptic analyses (Figure 4), calcium traces were smoothed by a gaussian filter with size = 1. Photostimulation targets coordinates were remapped into the stitched mesoscale FOV. and assigned to the closest suite2P identified calcium source.

Decoding photostimuli pairs

To discriminate between pairs of distinct photostimulation patterns, a gradient boosting decision tree algorithm was used. The classifier was trained on 70% of the trials (n=112 trials per pair labeled as either photostimulus 1 or photostimulus 2) and tested on the remaining trials (n = 48 trials). The decoding accuracy was defined as the number of correctly predicted trials over the total number of test trials. For each pair of photostimuli, the final reported decoding accuracy result was the average across 10 independent draws (cross-validation). For the shuffled control decoding, the classifier was trained on randomly mislabeled trials and tested on the 30% held-out trials.

Statistics

All statistical analyses were performed using Python or Matlab. The analyses performed were paired t-test, Wilcoxon sum-rank and Mann-Whitney U test and tests were two-sided. No statistical method was

561 used to predetermine sample size. Trial randomization was used in all applicable experiments (Figures
562 2,3,4).

563

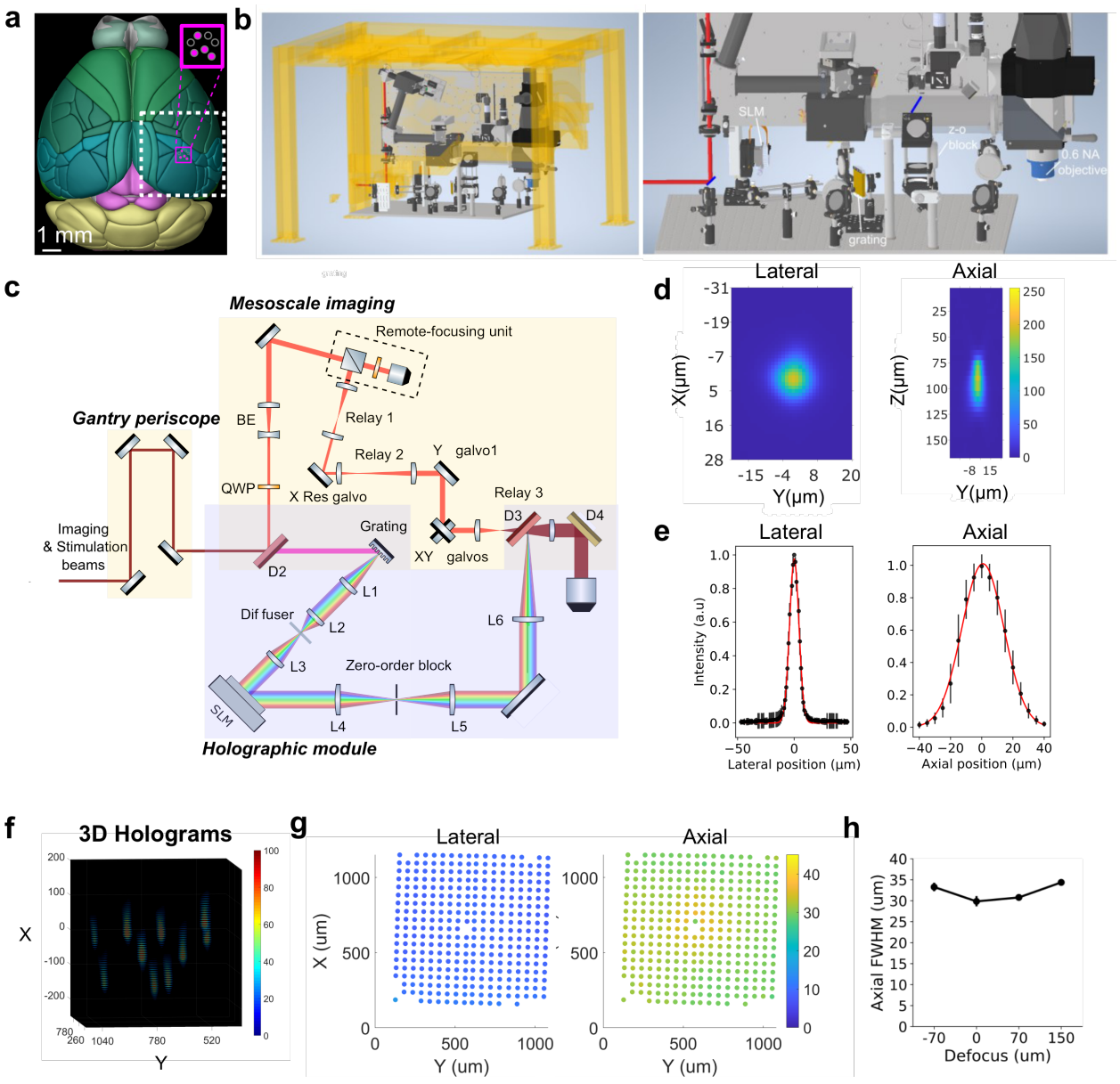

564

565 **Figure 1**. **A 2P-RAM mesoscope with temporally focused 2P holographic photostimulation**. **a)** Schematic
566 dorsal view of the mouse brain with putative functional areas demarcated (Allen Brain Explorer). The
567 holographic mesoscope allows targeted photostimulation in a 1x1 mm FOV (magenta square) combined
568 with simultaneous mesoscale imaging across a nominal 5x5 mm imaging FOV (dotted white). **b)** Left: CAD
569 model of the holographic mesoscope platform. Right: blow up of the holographic module attached to the
570 main frame of the mesoscope **c)** Simplified schematic of the optical path. QWP: quarter-wave plate, BE:
571 beam expander, Ln: achromatic doublet, Dn: dichroic mirror. **d)** Example lateral and axial 2P fluorescence
572 intensity profiles of a single, temporally focused holographic illumination spot. **e)** Optical lateral and axial
573 point-spread-functions (PSFs). Error bars: standard error of the mean (S.E.M). **f)** Example point-cloud 3D
574 holograms. **g)** 2D grid of single-spot holograms showing the extent of the holographic FOV and the
575 distribution of lateral and axial resolution across the FOV. **h.** Axial PSF as a function of digital Z-defocus.

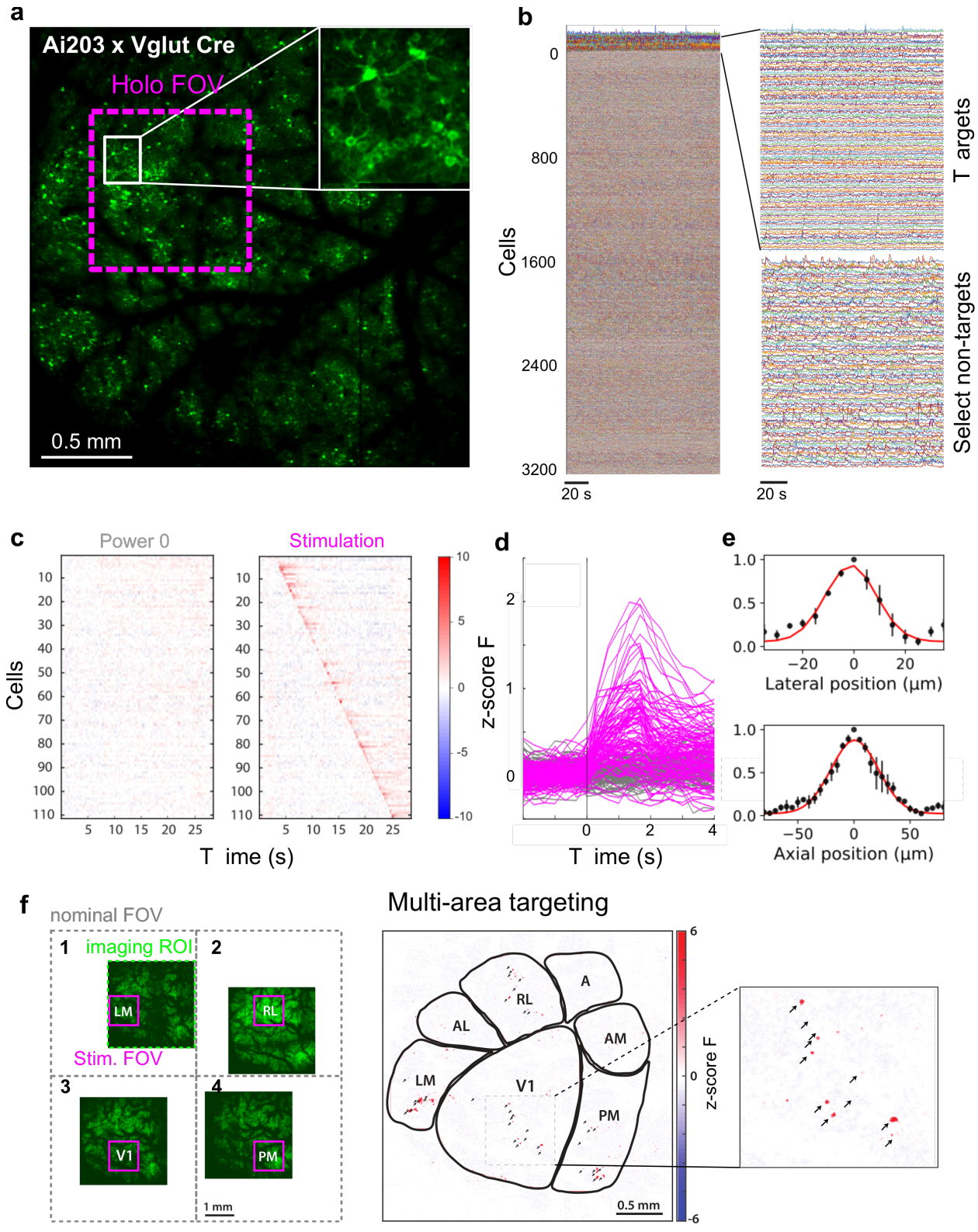

Figure 2. **Cellular resoltion two-photon holographic optogenetics at the mesoscale**. **a)** A 2p mesoscale image of widespread co-expression of GCaMP7s and ChroME over a large field-of-view (FOV) in an Vglut1-Cre;Ai203 transgenic mouse. Magenta square indicates the accessible holographic FOV within an example

mesoscale imaging FOV of 2.4 mm × 2.4 mm recorded at 4.5Hz frame rate. **b)** Example calcium traces from a set of photo-stimulation targets within the holographic FOV and thousands of traces from non-targets recorded across the mesoscale FOV. **c)** Calcium responses of targeted cells during single-cell sequential targeting on stimulation trials (right) vs. control trials without stimulation (left). **d)** Stimulus-aligned target cell responses across the holographic FOV (n=111 cells) **e)** *In vivo* optically measured physiological point-spread functions (n=3cells). Error bars: S.E.M. Red curve: Gaussian fit, lateral full-width-half-maximum (FWHM) 23 µm, axial FWHM: 49 µm. **f)** Demonstration of sequential area mesoscale holographic stimulation. Left: 4 example configurations to holographically target 4 different visual areas within the same session and record from surrounding visual areas. Imaging ROIs were selected for a 4.5 Hz imaging rate at 1µm/pixel. Center: Activation map of holographically targeted neurons in 4 visual areas (V1, PM, RL and LM). Black arrows point to target locations. Right: Zoomed in inset of the activation map in V1.

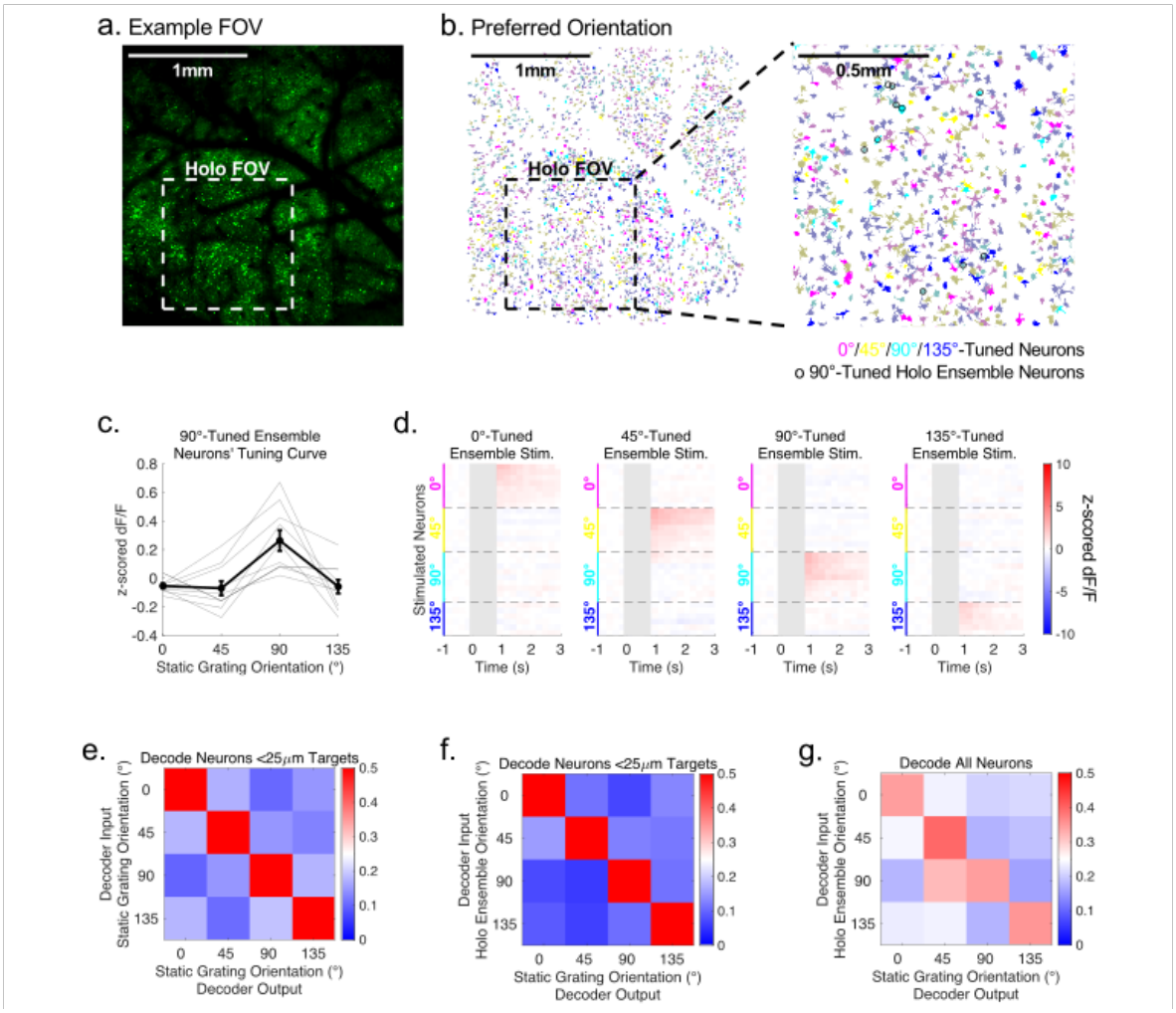

Figure 3. Holographic stimulation of co-tuned ensembles emulates visually evoked activity. **a)** Example imaging FOV used in this experiment (2.4 × 2.4 mm^2, Vglut1-Cre;Ai203 mouse). The holographic FOV was positioned over V1. **b)** Same FOV as **a**, with the cells color coded by their preferred orientation (0/45/90/135° in magenta/yellow/cyan/blue, respectively). Significantly tuned cells are labelled with solid colors while other cells are grayed out ($p<0.05$ Wilcoxon rank-sum test for preferred vs orthogonal orientations). Right: enlarged image of the holographic FOV with thin circles indicating the holographic targets that were activated by the 90°-tuned ensemble stimulation. **c)** Orientation tuning curves of a group of neurons that were then co-activated as the 90°-tuned ensemble stimulation in d). **d**) Holographically evoked activity in a population of neurons that were grouped into four distinct orientation-specific ensembles. Imaging frames recorded during the holographic stimulation are grayed out due to the holographic stimulation artifact. **e)** Classification accuracy of a linear support vector machine (SVM) trained to classify visual response of 4 orientations, for neurons within 25 μm of each target in holographic ensembles (average 77.7 neurons per session). 10-fold cross-validated decoding accuracy was 0.557 ± 0.019 mean ± standard error mean (SEM) across N=11 sessions ($p = 9.77 \times 10^{-4}$ Wilcoxon signed-rank test compared to chance-performance of 0.25). **f)** Classification accuracy of the same SVM when probed with orientation-specific holographically evoked activity without any visual stimulus (0.696 ± 0.043 mean ± SEM, $p = 9.77 \times 10^{-4}$ Wilcoxon signed-rank test across N=11 sessions). Decoding accuracy was

610 measured as the proportion of holography trials that were classified as the corresponding grating
611 orientation. **g)** As in f) but when using Linear SVMs trained on all neurons in the FOV (average 1865
612 neurons, 0.360 ± 0.026 mean ± SEM, $p = 9.77 \times 10^{-4}$ Wilcoxon signed-rank test across N=11 sessions).

613

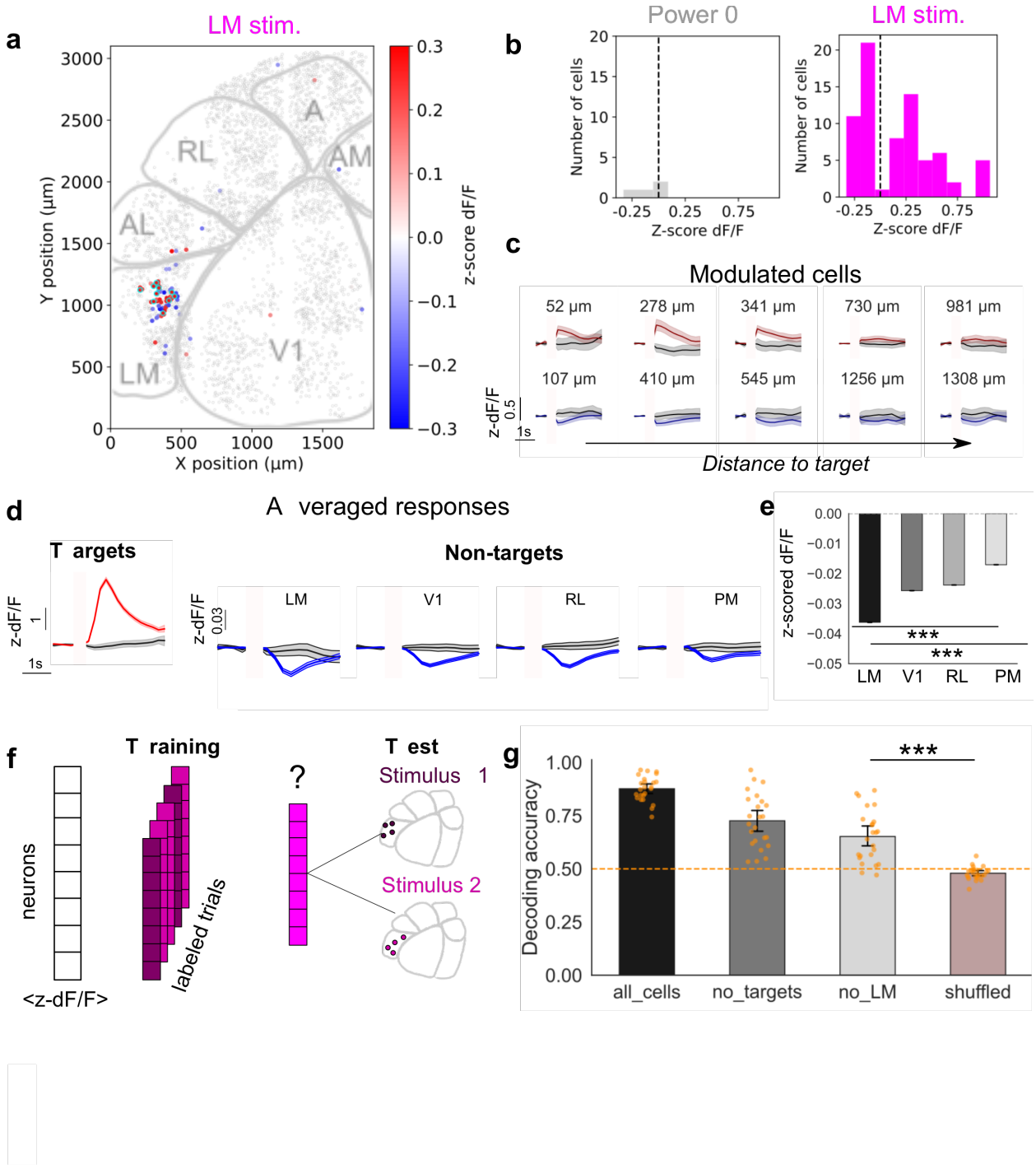

Figure 4. **Mesoscale recording of long-range, corticocortical responses to holographic activation**. **a)** An example mesoscale holographic 'influence' map measured in response to activation of an ensemble of LM neurons. Significantly modulated cells are colored according to the amplitude of their calcium responses. Non-modulated cells are displayed in gray. Holographic targets are circled in cyan. **b)** Distribution of the amplitude of the calcium responses post-stimulation compared to control trials with no stimulation. **c)** Example average calcium responses of individual modulated cells. Red/Blue: average response on stimulation trials (n=200 trials). Black: average response on control (no stimulation) trials (n=200 trials).

d-e) Average calcium responses across neurons in four areas (n=4 sessions, 2 mice) during multi-target (3-20 cells) stimulation in LM. Red/Blue traces: average across stimulation trials. Black traces: average across no-stimulation control trials. Mann-Whitney: LM/V1: 3.53E-20, LM/RL: 4.18E-24, LM/PM: 4.63E-59, V1/RL: 0.11, V1/PM: 8.66E-22, RL/PM:1.94E-17. **f)** Schematic of a decoder trained to discriminate different holographically induced patterns of activity from downstream responses. **g)** Decoding accuracy of a classifier trained to discriminate the holographically induced pattern in LM from different groups of non-targeted cells in the FOV. All_cells: decoding from all neurons in mesoscale FOV. No_targets: decoding from all neurons except the targeted cells. No_LM: decoding from all neurons outside area LM.